1      Characterizing chemical transformation of organophosphorus compounds by ^{13}C and ^{2}H stable

2      isotope analysis

3      Langping Wu[a], Barbora Chládková[a, b], Oliver J. Lechtenfeld [c], Shujuan Lian[a], Janine Schindelka[d],

4      Hartmut Herrmann[d], Hans H. Richnow[a,*]

5      [a] Department of Isotope Biogeochemistry, Helmholtz Centre for Environmental Research-UFZ,

6      Permoserstraße 15, 04318 Leipzig, Germany.

7      [b] Department of Polymer Engineering, Faculty of Technology, Tomas Bata University in Zlín,

8      Vavrečkova 275, 760 01 Zlín, Czech Republic, (Present address).

9      [c] Department of Analytical Chemistry, Helmholtz Centre for Environmental Research-UFZ,

10      Permoserstraße 15, 04318 Leipzig, Germany.

11      [d] Atmospheric Chemistry Department (ACD), Leibniz Institute for Tropospheric Research

12      (TROPOS), Permoserstraße 15, 04318 Leipzig, Germany.

13      *Email: hans.richnow@ufz.de, Tel: 0049 341 235 1212 Fax: 0341-450822

14      Abstract

15      Continuous and excessive use of organophosphorus compounds (OPs) has led to environmental

16      contaminations which raise public concerns. This study investigates the isotope fractionation

17      patterns of OPs in the aquatic environment dependence upon hydrolysis, photolysis and radical

18      oxidation processes. The hydrolysis of parathion (EP) and methyl parathion (MP) resulted in

19      significant carbon fractionation at lower pH (pH 2~7, $\varepsilon_C$=-6.9~-6.0‰ for EP, -10.5~-9.9‰ for

20      MP) but no detectable carbon fractionation at higher pH (pH 12). Hydrogen fractionation was

21    not observed during any of the hydrolysis experiments. These results indicate that compound

22    specific isotope analysis (CSIA) allows distinction of two different pH-dependent pathways of

23    hydrolysis. Carbon and hydrogen isotope fractionation were determined during UV/$H_2O_2$

24    photolysis of EP and tris(2-chloroethyl) phosphate (TCEP). The constant $\delta^2H$ values determined

25    during the OH radical reaction of EP suggested that the rate-limiting step proceeded through

26    oxidative attack by OH radical on the P=S bond. The significant H isotope enrichment suggested

27    that OH radical oxidation of TCEP was caused by an H-abstraction during the UV/$H_2O_2$

28    processes ($\varepsilon_H$ = -56 ±3‰). Fenton reaction was conducted to validate the H isotope enrichment

29    of TCEP associated with radical oxidation, which yielded $\varepsilon_H$ of -34 ±5‰. Transformation

30    products of OPs during photodegradation were identified using Fourier Transform Ion Cyclotron

31    Resonance Mass Spectrometry (FT-ICR MS). This study highlights that the carbon and hydrogen

32    fractionation patterns have the potential to elucidate the transformation of OPs in the

33    environment.

34    Key words: compound specific isotope analysis, parathion, TCEP, hydrolysis, photolysis,

35    transformation products.

36    **1. Introduction**

37    Organophosphorus compounds (OPs) are often used as pesticides, warfare agents, flame

38    retardants, plasticizers, or flotation agents. The OPs discussed in the present study are esters of

39    phosphoric acids, thiophosphoric acids and dithiophosphoric acids forming a wide variety of

40    phosphates, phosphorothioates, or phosphorodithioates (Fig. S1 in supplementary material (SM)),

41    each of them has different reactivity towards hydrolysis, oxidation and biodegradation

42    (Pehkonen and Zhang, 2002; Singh and Walker, 2006). Many OP derivatives are associated with

2

43     acute toxicity by inhibiting acetylcholinesterase (AChE) in the nervous system, hence they are

44     used as pesticides for control of insects and other higher organisms (Colovic et al., 2013). OP

45     pesticides are less persistent in the environment when compared with organochlorine pesticides

46     and thus have been widely used throughout the world. However, continuous and excessive use of

47     OPs has led to environmental contaminations which raise public concerns (EPA, 2006).

48     Parathion (*O,O*-diethyl *O*-(4-nitrophenyl) phosphorothioate), also known as ethyl parathion (EP),

49     was one of the most widely applied organophosphorus insecticides in agriculture in the past

50     decades, and was primarily used as an insecticide on fruit, cotton, wheat, vegetables, and nut

51     crops (FAO, 1990b). The average half-life time of EP during hydrolysis, degradation in aerobic

52     soil and anaerobic soil are 302 days, 58 days and 21 days respectively (Kegley et al., 2016b),

53     which leads to a huge potential for EP and its metabolic products to contaminate surface water

54     and groundwater. Its use is banned or restricted in many countries but continues in many other

55     developing countries including China and India, where the application is still legal for crops.

56     Methyl parathion (*O,O*-dimethyl-*O*-(4-nitrophenyl) phosphorothioate, MP) is structurally very

57     similar to EP and less persistent in the environment, with an average half-life time during

58     hydrolysis, degradation in aerobic soil and anaerobic soil of 45 days, 12 days and 1 day,

59     respectively (Kegley et al., 2016a). Due to its severe hazardous potential classified by the

60     Rotterdam Convention, MP is not allowed for sale and import in nearly all countries around the

61     world (RotterdamConvention, 2004).

62     Tris(2-chloroethyl) phosphate (TCEP) is an anthropogenic organic compound used as flame

63     retardant, plasticizer, and viscosity regulator in various types of polymers, and is commonly

64     listed among a class of emerging contaminants associated with wastewater pollution of

3

65   freshwater resources (Andresen et al., 2004; Stackelberg et al., 2007). TCEP is considered as

66   almost non-biodegradable and not expected to hydrolyze significantly under environmental

67   conditions, thus advanced oxidation processes (AOP), such as Fenton reaction and $UV/H_2O_2$,

68   have been studied as a possible remediation strategy (Ou et al., 2017; Watts and Linden, 2008;

69   Watts and Linden, 2009; Yuan et al., 2015).

70   Compound specific stable isotope analysis (CSIA) can provide additional information on the

71   organic pollutants' transformation pathways in complex environments (Elsner et al., 2005;

72   Hofstetter and Berg, 2011; Thullner et al., 2012). Previous studies have shown the potential use

73   of stable isotope fractionation to characterize transformation mechanisms of organic compounds

74   (Elsner, 2010; Elsner and Imfeld, 2016; Elsner et al., 2012; Nijenhuis and Richnow, 2016; Vogt

75   et al., 2016; Wu et al., 2014), as this approach is a valuable tool to analyze the rate-limiting step

76   in reaction mechanisms such as the mode of chemical bond cleavage (Northrop, 1981).

77   Hydrolysis is one pathway controlling the fate of OPs in the environment and react by a common

78   mechanism, where $H_2O$ and $OH^-$ act as nucleophiles in a bimolecular nucleophilic substitution

79   mechanism ($S_N2$ mechanism) (Pehkonen and Zhang, 2002). The esters of phosphates,

80   phosphorothioates, and phosphorodithioates can be hydrolyzed under acidic and alkaline

81   conditions by two different pathways but the relative contribution of each hydrolysis pathway is

82   pH-dependent. Photodegradation and chemical oxidation are other important degradation

83   processes. Several studies investigated the reaction mechanisms of OPs during photodegradation,

84   in which simultaneous pathways including oxidation of P=S to P=O, elimination of nitro group,

85   remethylation and oxidation of the alkyl substituent were proposed (Araújo et al., 2007; Durand

86   et al., 1994; Kanmoni et al., 2012; Sakellarides et al., 2003; Santos et al., 2005; Wu and Linden,

87   2008). Although several types of transformation products were typically determined, it is

4

88  difficult to confirm photodegradation pathways via identified transformation products, as short-

89  lived intermediates could be missed.

90  Previous studies reported OPs contamination in natural waters (Pehkonen and Zhang, 2002) and

91  atmosphere (Kawahara et al., 2005). OP residues have been found in rain, snow, fog and air

92  samples (Aston and Seiber, 1996). Oxidation of OPs by OH radical is likely in surface water and

93  atmosphere (aerosols). OH radical can be generated by natural presented photosensitizers such as

94  humic substances (Zhang et al., 2015). The photosensitizers promoted indirect photolysis is a

95  naturally occurring degradation process. It may be an important factor governing the fate of

96  organic contaminants in the environment. The multi-isotope fractionation pattern allows

97  characterize the bond cleavage mechanisms of photosensitization, and is thus a valuable tool for

98  studying the fate of OPs in surface waters and atmospheric media containing photosensitizers.

99  The main objective of this study is to evaluate the carbon and hydrogen isotope fractionation

100  patterns associated with hydrolysis and photolysis which are considered to be important chemical

101  transformation reactions of OPs in the environment. We selected EP, MP and dimethoate (Wu et

102  al., 2017) as model compounds of phosphorothioates and phosphorodithioates representing

103  typical esters of phosphoric acids  and analyzed the carbon and hydrogen isotope fractionation

104  patterns upon hydrolysis at various pH values to study the different mode of hydrolysis by CSIA.

105  Radical oxidation and photolysis of EP (model of phosphorothioates) were investigated to

106  compare isotope fractionation patterns with those obtained from hydrolysis. In addition, OH

107  radical oxidation of TCEP (model of phosphate) by Fenton reaction (the iron catalyzed hydrogen

108  peroxide) and via indirect photolysis (UV/$H_2O_2$) was performed to understand the isotope

109  fractionation associated by an H-abstraction step. The transformation products were further

110 identified using Fourier Transform Ion Cyclotron Resonance Mass Spectrometry (FT-ICR MS)

111 to analyze the transformation mechanisms.

112 **2. Materials and methods**

113 2.1 Chemicals

114 Parathion (*O, O*-diethyl *O*-(4-nitrophenyl) phosphorothioate, purity > 99.7%), methyl parathion

115 (*O, O*-dimethyl-*O*-(4-nitrophenyl) phosphorothioate; purity>99.8%), TCEP (tris(2-chloroethyl)

116 phosphate, purity> 97.0%) and dichlorvos (2,2-dichlorovinyl dimethyl phosphate, purity >

117 98.8%) were purchased from Sigma-Aldrich (Munich, Germany) and used without further

118 purification. Tributyl phosphate (TBP, purity 99%) was purchased in Xiya Company in China.

119 Hydrogen peroxide (30% w/w) was supplied by Merck (Darmstadt, Germany).

120 2.2 Hydrolysis experiment

121 Hydrolysis of EP and MP were carried out at up to 60°C (to reduce the reaction time) in 100 mM

122 phosphate buffer solution at pH 2, pH 5, pH 7, pH 9 and pH 12, respectively. All experiments

123 were conducted as batch experiments in 100 mL buffer solution, with an initial concentration of

124 24 mg L$^{-1}$ for EP and 50 mg L$^{-1}$ for MP. At different time intervals, the hydrolysis was stopped

125 by adjusting the whole 100 mL aquerous sample to pH 7 using 6N HCl or 5M NaOH. The

126 residues of EP and MP were extracted by 2 mL dichloromethane containing 400 mg L$^{-1}$ of

127 dichlorvos as internal standard, shaking at 180 rpm for 2h. Afterwards, the organic phase was

128 transferred into 2mL vials for concentration and isotope analysis.

129 2.3 Direct photolysis and OH radical reaction

6

130     The photolysis of EP was conducted in a photochemical reactor system consisting of a 2 L Pyrex

131     cylindrical flask and a circulating water system. Irradiation was achieved using a 150-W xenon

132     lamp as the light source (Type L2175, wavelength: 185-2000 nm, Hamamatsu, Japan). The light

133     spectrum is shown in Fig. S2. A filter with a 280 nm cut-off wavelength (Schott WG 280 long

134     pass filter, 3.15mm thick, Galvoptics Ltd, United Kingdom) was applied to provide emission

135     spectrum with wavelengths $\geq$280 nm typical of the sun at the Earth's surface. All EP experiments

136     were conducted in phosphate buffer (10 mM, pH 7) at 25 °C, with initial concentration of 10 mg

137     $L^{-1}$. For the OH radical oxidation experiments, 30% $H_2O_2$ was used to obtain initial molar ratio

138     of $H_2O_2$: EP to 500:1. The direct photolysis of EP was performed at the same conditions without

139     $H_2O_2$ and without 280 nm filter as EP has maximum absorption at 277 nm in MilliQ water and

140     maximum absorption at 289 nm in phosphate buffer (Fig. S3). Dark control experiments were

141     conducted in the same system without UV irradiation.

142     The OH radical reaction of TCEP was conducted in the same photochemical reactor system as

143     for EP, but using a 200 mL Pyrex cylindrical flask. All TCEP experiments were conducted in

144     phosphate buffer (100 mM, pH 7) at 20 °C, with initial concentration of 500 mg $L^{-1}$, 30% $H_2O_2$

145     was used obtain initial molar ratio of $H_2O_2$: TCEP to 50:1. Dark control experiments were

146     conducted in the same system without UV irradiation in order to investigate the oxidation of

147     TCEP by $H_2O_2$. Another control experiment was performed at the same condition but without

148     $H_2O_2$ in order to investigate the direct photolysis of TCEP. More detailed information is

149     described in SM.

150     2.4 Fenton reaction

151    The OH radical oxidation by Fenton reaction of TCEP was investigated at room temperature in

152    200 mL well-stirred phosphate buffer (100 mM, pH 3) with an initial molar ratio of

153    $TCEP:H_2O_2:FeSO_4$ to 1:50:10. The initial concentration of TCEP was 500 mg $L^{-1}$. To attain

154    homogeneous reaction, required amount of TCEP and $Fe^{2+}$ stock solution was first dissolved into

155    buffer and stirred for 30 min. The Fenton reaction was then initiated by sequential addition of 1.8

156    mL of 30% $H_2O_2$ (30min sequencing intervals). The solution was continuously mixed at 400 rpm

157    during 2-hour reaction. At 30 min intervals, 10 mL of aqueous sample was taken for the

158    extraction of TCEP residues by adding 0.5 mL of dichloromethane containing 2000 mg $L^{-1}$ TBP

159    as internal standard and shaken at 180 rpm at 4 °C for 2h. The excessed OH radicals were

160    quenched by an addition of 1 mL of isopropanol to stop the reaction during extraction procedure.

161    2.5 Analytical methods

162    2.5.1 Concentration determination

163    An Agilent 6890 series GC (Agilent Technologies, USA) equipped with a flame ionization

164    detector (FID) was used to determine the concentration throughout the study. Analytes were

165    separated in an HP-5 column (30 m × 320 μm × 0.25 μm, Agilent 19091J-413, USA) with

166    helium flow of 1.5 mL $min^{-1}$ as the carrier gas. The oven was first held at 60 °C for 2 min, then

167    increased at 10 °C $min^{-1}$ to 160 °C, at 5 °C $min^{-1}$ to 220 °C, and finally at 15 °C $min^{-1}$ to 280 °C

168    and held for 2 min. Each TCEP sample containing internal standard was measured once with a

169    split ratio of 50:1, EP and MP samples were measured with a split ratio of 10:1.

170    2.5.2 Isotope analysis

8

171 The carbon and hydrogen isotope compositions were analyzed by gas chromatograph-

172 combustion-isotope ratio mass spectrometer (GC-C-IRMS) and gas chromatograph-chromium

173 based high temperature conversion-isotope ratio mass spectrometer (GC-Cr/HTC-IRMS) system

174 using the same methods as described by Wu and colleagues (Wu et al., 2017) but with

175 modifications on oven temperature programs: the column was initially held at 60 °C for 2 min,

176 ramped at 8 °C min$^{-1}$ to 280 °C, and then held for 2 min. All samples were run in triplicates and

177 errors are reported in SM. All hydrogen isotope results were calibrated by two-point calibration

178 against two reference compounds using hexadecane A ($\delta^2$H = -167 ‰) and hexadecane B ($\delta^2$H =

179 -11‰) which were described elsewhere (Renpenning et al., 2015). The quantification of isotope

180 fractionation was evaluated by isotope enrichment factors ($\varepsilon$) using Rayleigh equation which is

181 reported previously (Elsner et al., 2005; Hofstetter et al., 2008) and described briefly in SM.

182 2.5.3 Transformation product analysis

183 Transformation products of EP and TCEP during photodegradation were tentatively identified

184 analyzing the precise mass via ultra-high resolution FT-ICR MS (Solarix XR 12T, Bruker

185 Daltonics) based on accurate masses allowing calculating elemental compositions of ions. 10 mL

186 of aqueous solution was extracted by solid phase extraction (SPE) using Bond Elut PPL

187 cartridges (50 mg, Agilent). The SPE extraction procedures followed the manufacturer

188 guidelines and the transformation products were eluted with 0.5 mL methanol. The methanolic

189 extract was diluted 1:100 or 1:1000 (v/v) with MilliQ water /MeOH (1:1, v/v) before analysis. A

190 FT-ICR MS equipped with a dynamically harmonized analyzer cell was used for the analysis of

191 the methanolic extracts. Samples were measured with positive and negative mode electrospray

192 ionization in direct infusion mode with a 4 MWord time domain using typical electrospray

193 ionization (ESI) conditions. For each sample, 16 (TCEP) or 128 to 256 scans (EP, 10 – 100 ms

194    ion accumulation time) were co-added in a range of 73-3000 m/z and the spectra externally

195    calibrated with <mark>fatty acids present in the samples between m/z 83 and m/z 353.</mark> The high mass

196    accuracy and resolution (450000 at m/z 200) allowed for a tentative assignment of possible

197    transformation products via their exact mass and calculated molecular formulas where the

198    molecular formulas of the parent compounds were used as an upper element limit for the

199    calculation. For further method details, refer to the SM.

## 3. Results and discussion

201    3.1 Isotope fractionation patterns of EP and MP during hydrolysis

202    More than 90% of MP and EP were hydrolyzed in phosphate buffer at pH 2 ~ 12 and C and H

203    isotope ratios were analyzed (Fig.1). The hydrolysis of MP and EP is a homogeneous reaction

204    following pseudo-first-order kinetics (Fig. S6), the rate constants under all examined conditions

205    are shown in Table 1. As shown in Fig. 1, significant C isotope fractionation was observed

206    during MP hydrolysis at lower pH and could be quantified by the Rayleigh model, corresponding

207    to isotope enrichment factors of $\varepsilon_C = -10.0 \pm 0.7‰$ at pH 2, $\varepsilon_C = -10.5 \pm 1.1‰$ at pH 5 and $\varepsilon_C = -$

208    $9.9 \pm 0.7‰$ at pH 7. The C isotope fractionation upon EP hydrolysis corresponding to isotope

209    enrichment factors of $\varepsilon_C = -6.9 \pm 0.8‰$ at pH 2, $-6.7 \pm 0.4‰$ at pH 5 and $-6.0 \pm 0.2‰$ at pH 7

210    were described by the Rayleigh model as well. Smaller but significant C isotope fractionation

211    corresponding to isotope enrichment factor of $\varepsilon_C = -6.5 \pm 0.4‰$ for MP and $\varepsilon_C = -3.5 \pm 0.4‰$ for

212    EP were observed during hydrolysis at pH 9, however, no C isotope fractionation was observed

213    for both MP and EP hydrolysis at pH 12, indicating a different pathway.

214    The reduction of C isotope fractionation by almost <mark>50 %</mark> at pH 9 suggests <mark>compared to neutral</mark>

215    <mark>conditions</mark> that two pathways of hydrolysis take place. If a substrate is being degraded via two

216  competing pathways and following first-order kinetics, the rate ratio (F) of two competing

217  pathways can be calculated from the observed isotope enrichment factor and the isotope

218  enrichment factors associated with the two pathways. The extended Rayleigh-type equation

219  derived by Van Breukelen (Van Breukelen, 2007) was employed to calculate the contribution of

220  each pathway. According to the calculation (described in SM), MP hydrolysis at pH 9 has a

221  contribution of 62 ~ 66% compared to the reaction pathway under acidic condition, while EP

222  hydrolysis at pH 9 has a contribution of 51 ~ 58% compared to the pathway under acidic

223  condition.


224  Furthermore, we did not observe significant changes in H isotope ratios of MP and EP during

225  hydrolysis at any pH, indicating no H bond cleavage is involved during the rate limiting step of

226  the hydrolysis. The combination of negligible H and significant C isotope fractionation indicates

227  that hydrolysis under acidic and neutral conditions undergoes the same transformation

228  mechanism which involves C bond cleavage. Transformation mechanism changes under strong

229  alkaline condition, suggesting no C bond cleavage in the rate limiting step at pH 12. Thus, C

230  isotope fractionation can be used to distinguish different types of hydrolysis of MP and EP. The

231  observed similar isotope fractionation patterns during the hydrolysis suggest the same

232  transformation mechanisms for MP and EP. The smaller $\varepsilon_C$ obtained in EP hydrolysis at the same

233  pH can be explained by isotope dilution effects, as EP molecules contain two more carbon atoms

234  in comparison to MP molecules.

235

236
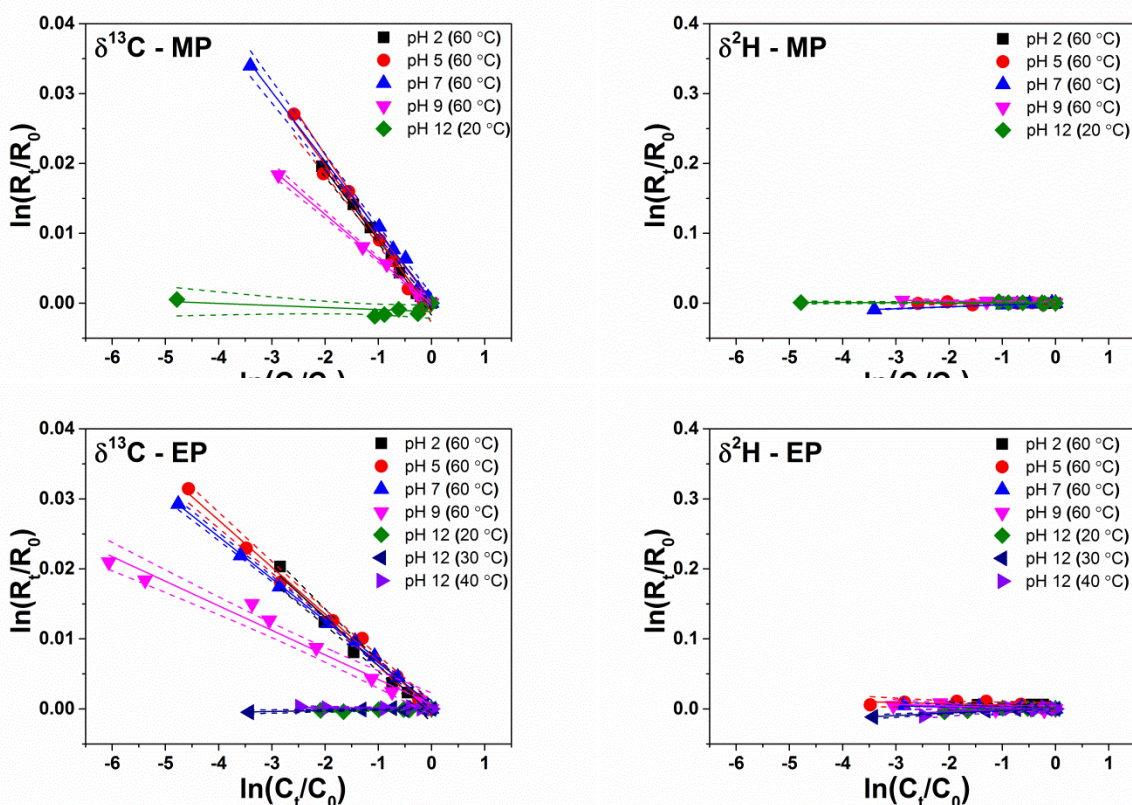
Fig. 1. Rayleigh plots for Carbon and hydrogen stable isotope fractionation of EP and MP during

hydrolysis at different pH. Dashed lines indicate the 95% confidence intervals. The ε values were

reported in Table 1.

3.2 Exploring the hydrolysis mechanisms of OPs

General hydrolysis pathways of OPs were proposed in Scheme 1. Two pathways have been

reported previously for EP hydrolysis (Wanamaker et al., 2013). The previous reported pathways

can be characterized by isotope fractionation analysis. Under acidic/neutral conditions, the

product O-ethyl O-(4-nitrophenol) hydrogen phosphorothioate is formed through C-O bond

cleavage, which results in a significant C isotope enrichment. The major transformation products

of 4-nitrophenol and O, O-diethyl hydrogen phosphorothioate at higher pH suggest a P-O bond

12

247 cleavage which supports our interpretation that no C isotope fractionation is observed at pH 12

248 due to no C bond cleavage in the rate limiting step of the reaction. An enrichment factor of $\varepsilon_C$ = -

249 3.5 ± 0.4‰ obtained during hydrolysis at pH 9 indicates that two hydrolysis pathways of EP are

250 active simultaneously. The P-O bond cleavage has no effect on isotope composition of EP and

251 lower the isotope fractionation contributed from the O-C bond cleavage mechanism. No H

252 isotope fractionation is observed during EP hydrolysis at any pH since no H bond cleavage is

253 involved in the rate determining step of the first irreversible reaction.

254 The similar hydrolysis pathways are reported for MP, where the dominant product of acid

255 hydrolysis is O-methyl O-(4-nitrophenol) hydrogen phosphorothioate while under alkaline

256 hydrolysis the main product is 4-nitrophenol (FAO, 1990a). The interpretation of the reaction

257 mechanisms suggested in former studies appears to be consistent with the isotope fractionation

258 results of the present study: O-methyl O-(4-nitrophenol) hydrogen phosphorothioate is formed

259 through C-O bond cleavage during acid hydrolysis, leading to significant C isotope enrichment

260 in the remaining phase; 4-nitrophenol is produced through P-O bond cleavage during alkaline

261 hydrolysis and gives no C isotope fractionation. The same hydrolysis pathways were investigated

262 using isotope fractionation for dimethoate in a previous study from our laboratory (Wu et al.,

263 2017), where the enrichment factor of $\varepsilon_C$ = -8.3 ± 0.3‰ at pH 7 indicated a C–O bond cleavage;

264 and a P–S bond cleavage at pH 12 resulted in a negligible enrichment factor of $\varepsilon_C$ = -0.4 ± 0.1‰.

265 In summary, we propose two general hydrolysis pathways of OPs including phosphates,

266 phosphorothioates and phosphorodithioates (Scheme 1): one is P-O (S) bond cleavage by

267 nucleophilic attack at the phosphorus atom, resulting in no C (and H) isotope fractionation;

268 another one is C-O bond cleavage by nucleophilic attack at the carbon atom, resulting in a

269  significant C (and no H) isotope fractionation. Therefore, C isotope fractionation can be used to

270  distinguish different hydrolysis pathways of OPs.
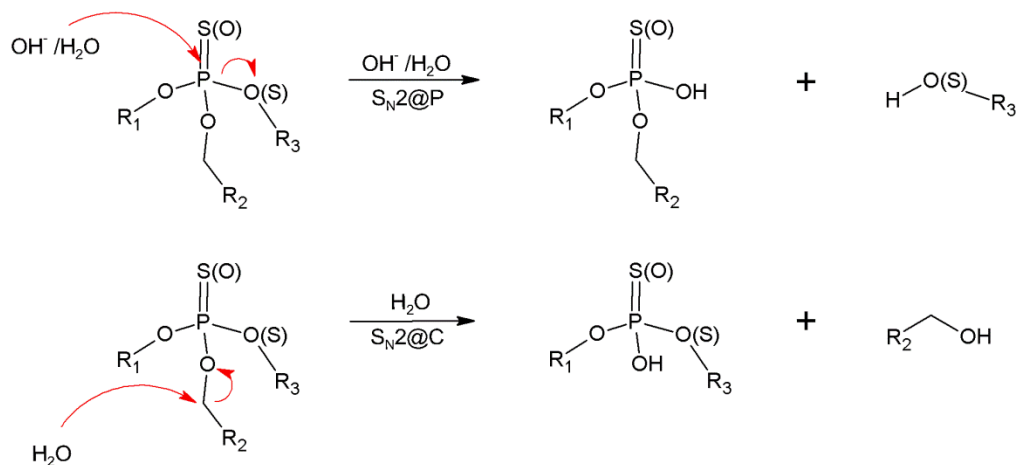


272  Scheme 1. Proposed transformation mechanisms of OPs during hydrolysis at different pH.

273  Hydrolysis of OPs can occur via two pathways: attack by $OH^-$ and $H_2O$ at the phosphorus atom

274  at high pH and attack by $H_2O$ at the α-carbon of the alkoxy group at low pH. $R_1$ and $R_2$ are

275  predominantly aryl or alkyl group. $R_3$ can be diverse and may belong to a wide range of aliphatic,

276  aromatic or heterocyclic group.

277  3.3 Isotope fractionation patterns of EP during direct photolysis and OH radical reaction

278  EP shows a maximum absorption at 289 nm when dissolved in phosphate buffer (Fig. S3). Up to

279  99% of EP was converted slowly after 359 h during direct photolysis without applying a 280 nm

280  cut-off filter. The same amount of EP was transformed much faster, within 23 h, during the

281  indirect photolysis (UV/$H_2O_2$) at wavelengths above 280 nm. The obtained rate constants of 0.36

282  $\times 10^{-5}$ $s^{-1}$ with $R^2$ of 0.976 for direct photolysis and 4.61 $\times 10^{-5}$ $s^{-1}$ with $R^2$ of 0.992 for indirect

283  photolysis indicate that photolysis and the OH radical oxidation of EP follows pseudo-first-order

284  kinetics (Fig. S8). C isotope fractionation associated with direct photolysis and OH radical

14

285 reaction of EP was low but still could be quantified by the Rayleigh model. The $\delta^{13}C$ was

286 enriched by 2.8‰ after more than 99% of EP degradation during direct photolysis,

287 corresponding to a $\varepsilon_C$ of $-0.6 \pm 0.1$‰ (Fig. 2). The $\delta^{13}C$ only enriched by 1.5‰ after more than

288 98% of EP conversion during OH radical oxidation induced by $UV/H_2O_2$ photolysis,

289 corresponding to a $\varepsilon_C$ of $-0.8 \pm 0.1$‰ (Fig. 2). No detectable H isotope fractionation was

290 observed during both experiments of EP, suggesting no H bond breaking occurs.
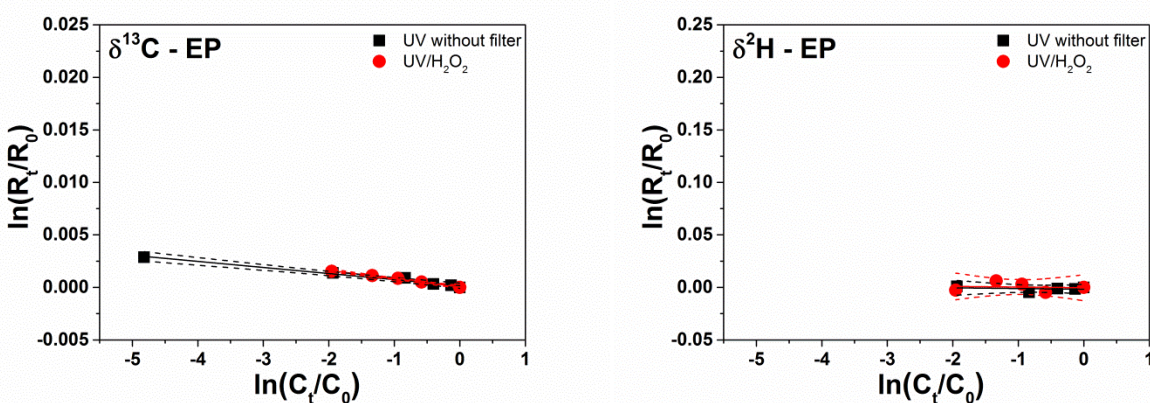
291


292 Fig. 2. Rayleigh plots for carbon and hydrogen stable isotope fractionation of EP during direct

293 photolysis (without filter) and OH radical reaction ($UV/H_2O_2$). Dashed lines indicate the 95%

294 confidence intervals. No hydrogen isotope fractionation was obtained. The $\varepsilon_C$ values were

295 reported in Table 1.

296 3.4 Isotope fractionation patterns of TCEP during OH radical reaction

297 TCEP is transparent in the wide range of 200 – 800 nm wavelengths (Fig. S3) and thus has no

298 potential to harvest light for direct photolysis. The OH radical oxidation and corresponding C

299 and H isotope fractionation of TCEP was investigated using $UV/H_2O_2$ and Fenton reagents

300 $FeSO_4/H_2O_2$, respectively. In the $UV/H_2O_2$ system, the $\delta^{13}C$ value of TCEP was enriched

301  from -31.5 ± 0.2‰ to -26.3 ± 0.3‰ after 13 h (97% of degradation) and $\delta^2$H value was enriched

302  from -25 ± 5‰ to 185 ± 5‰ (Fig. S9). Rate constant of 7.86 ×$10^{-5}$ $s^{-1}$ with $R^2$ of 0.999 indicates

303  a pseudo-first-order kinetic reaction (Fig. S8). The C and H isotope fractionation can be

304  quantified by the Rayleigh equation yielding a small $\epsilon_C$ of −1.4 ± 0.1‰, and a large $\epsilon_H$ of −56 ±

305  3‰. The hydrogen and carbon fractionation are linearly correlated yielding a dual isotope

306  enrichment factor ($\Lambda$) of 43 ± 5 (Fig. 3). $\Lambda$ is the slope of the linear relationship of isotope

307  composition shifts of both elements ($\Delta\delta^2$H vs $\Delta\delta^{13}$C), expressed as $\Lambda = \Delta\delta^2\text{H}/\Delta\delta^{13}\text{C}$, where

308  $\Delta\delta^2\text{H} = \delta^2\text{H}_t - \delta^2\text{H}_0$, $\Delta\delta^{13}\text{C} = \delta^{13}\text{C}_t - \delta^{13}\text{C}_0$. The control experiment without adding $H_2O_2$ clearly

309  showed no loss of TCEP after 136 h, indicating that no direct photolysis of TCEP occurred.

310  Fenton reaction of TCEP is a pseudo-first-order kinetic reaction too. The $\delta^{13}$C value was

311  enriched from -29.4 ± 0.3‰ to -26.2 ± 0.2‰ and $\delta^2$H was enriched from -28 ± 3‰ to 87 ± 4‰

312  after 96% degradation (Fig. S9), yielding a fractionation factor of $\epsilon_C$ of −1.0 ± 0.2‰ and $\epsilon_H$ of

313  −34 ± 5‰. The hydrogen and carbon fractionation are linearly correlated by a $\Lambda$ factor of 35 ± 5

314  (Fig. 3).

315

316
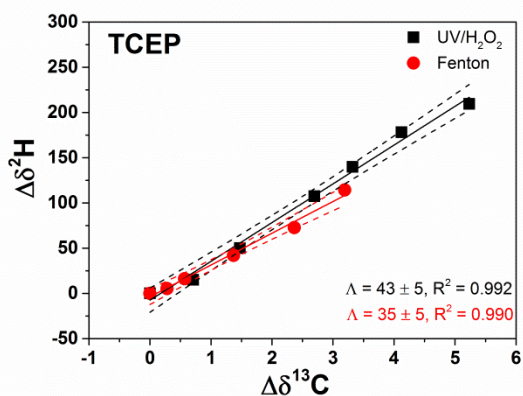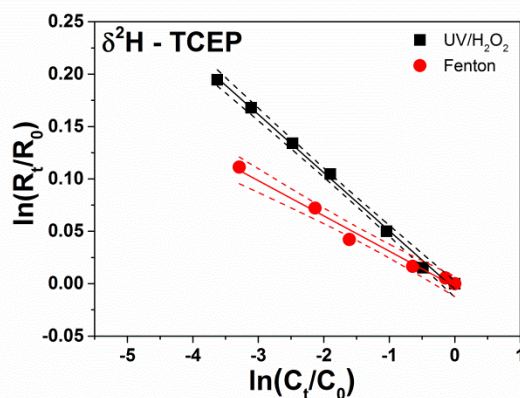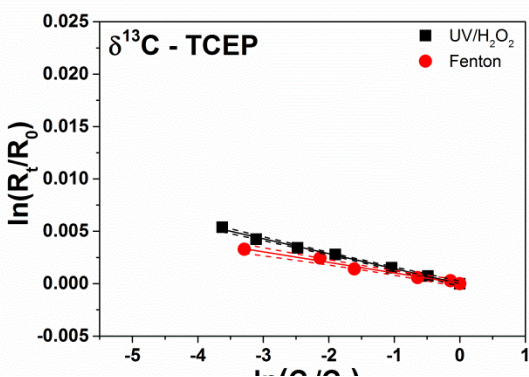
Fig. 3. Rayleigh plots quantifying $^2$H and $^{13}$C fractionation of TCEP and the correlation of $^2$H

and $^{13}$C fractionation during OH radical oxidation by UV/H$_2$O$_2$ and Fenton reaction. Dashed

lines indicate the 95% confidence intervals. The $\varepsilon_C$ and $\varepsilon_H$ values were reported in Table 1.

3.5 Exploring the OH radical reaction mechanisms of OPs

The FT-ICR MS analysis was used to identify photodegradation products of EP and TCEP to

confirm proposed OP transformation pathways using transformation products patterns.

Photodegradation of EP yielded five major transformation products (Table S1). The rate-limiting

step of photodegradation of EP involves OH radical addition to the central phosphorus atom to

yield an phosphorenyl radical, this OH adduct radical may be prone to stabilization by two

different pathways as illustrated in Scheme 2a: (A) stabilization by the elimination of sulfhydryl

17

327  radical to produce P=O bond to form Paraoxon (P1) ($C_{10}H_{14}NO_6P$, m/z pos: 276.0632) which was

328  one of the major products determined in the reaction solution. Previous studies shows that the

329  oxidative attack of the OH radicals on the P=S bond occurs firstly in the case of

330  phosphorothioates, such as dichlofenthion (Konstantinou et al., 2001), pirimiphos-methyl

331  (Herrmann et al., 1999), fenitrothion (Kerzhentsev et al., 1996) and dimethoate (Evgenidou et al.,

332  2006). Wu and colleagues studied desulfurization of phosphorothioate and proposed that the

333  sulfur atom can be replaced by an oxygen atom via a radical mechanism (Wu et al., 2012). (B)

334  Stabilization by the elimination of nitrophenol from the phosphoric center to form P2 ($C_6H_5NO_3$,

335  m/z neg: 138.0197) and P3 ($C_4H_{11}O_3PS$, m/z neg: 169.0094). The subsequent reaction of

336  Paraoxon (P1) may lead to the formation of P2 and P4 ($C_4H_{11}O_4P$, m/z neg: 153.0322) through a

337  P-O bond cleavage.

338  Transformation product analysis showed no difference between direct photolysis and OH radical

339  oxidation of EP, indicating the same transformation mechanisms starting with the oxidation of

340  the sulfur. The proposed mechanisms are consistent with isotope fractionation results, as no

341  significant C or H isotope fractionation was observed (Fig. 2). Wu and Linden proposed a third

342  pathway where a hydroxyl radical attacks the nitrophenyl bond which results in a formation of

343  O,O-diethyl-phenyl thiophosphate (Wu and Linden, 2008). The observed $\epsilon_C$ of -0.6 ± 0.1‰ from

344  direct photolysis and $\epsilon_C$ of -0.8 ± 0.1‰ from OH radical oxidation (Fig. 2, Table 1) are too small

345  to be indicatives of C-N bond cleavage. In addition, P5 (O,O-diethyl phenyl thiophosphate,

346  $C_{10}H_{15}O_3PS$) with expected m/z pos: 247.0552 or m/z neg: 245.0407 was not detected as a

347  transformation product by FT-ICR MS analysis in the present study.

348  Eight transformation products (P1 to P8) were detected in the photodegradation of TCEP using

349  UV/$H_2O_2$, the tentative structure of the products are shown in Table S2. Scheme 2b illustrates the

350    proposed first step transformation of TCEP during OH radical reaction. Pathway A involves

351    hydrogen abstraction from the alkyl-C position by OH radical to produce carbon-centered radical,

352    which is followed by oxygen addition to generate the peroxyl radical. Peroxyl radicals typically

353    undergo a bimolecular Russell Mechanism (Miyamoto et al., 2003) leading to the corresponding

354    alcohol, P1 ($C_6H_{12}Cl_3O_5P$, m/z pos (Na): 322.9380), and aldehyde which are expected to be

355    readily hydrolyzed to P2 ($C_6H_{11}Cl_2O_6P$, m/z neg: 278.9598). Pathway B involves OH radical

356    addition to the central phosphorus atom to yield an oxygen-centered phosphorenyl radical, which

357    is followed by the elimination of an ethyl-chlorine arm from the phosphoric center to form P3

358    ($C_4H_9Cl_2O_4P$, m/z neg: 220.9543). In addition, P4 ($C_6H_{13}Cl_2O_5P$, m/z neg: 264.9805) was detected

359    with a lower intensity compared to other transformation products, which is likely formed by the

360    hydrolysis of TCEP resulting a substitution of one chlorine terminal by a carboxyl. Further

361    breakdown products formed in subsequent reactions are found (P5 to P8 see SM) which are not

362    discussed in this study.

363    Hydrogen abstraction and addition-elimination are the primary mechanisms for the

364    photocatalytic oxidation of dimethyl methylphosphonate (DMMP) via hydroxyl radical attack

365    (Aguila et al., 2001; Oshea et al., 1997). Similar mechanisms are proposed for the degradation of

366    TECP via persulfate radical attack (Ou et al., 2017). The significant isotope fractionation of

367    TCEP of $\varepsilon_H = -56 \pm 3‰$ combined with $\varepsilon_C = -1.4 \pm 0.1‰$ suggests a C-H bond cleavage, which

368    supports the H abstraction mechanism as well.

369    Our results suggest that the major reaction mechanisms of OPs during OH radical reaction are

370    related to their chemical structures as illustrated in Scheme 2: (1) The P=S bond is oxidized to

371    P=O in case of phosphorothioate structure (e.g. EP) in the rate determining step yielding very

372    low or no carbon and hydrogen fractionation in contrast to (2) C-H bond breaking through H

19

373 abstraction step in case of phosphate structure substitution by alkyl groups (e.g. TCEP). These

374 two major chemical structures-dependent reaction mechanisms of OPs can be distinct when

375 applying C and H isotope fractionation approach diagnostically.
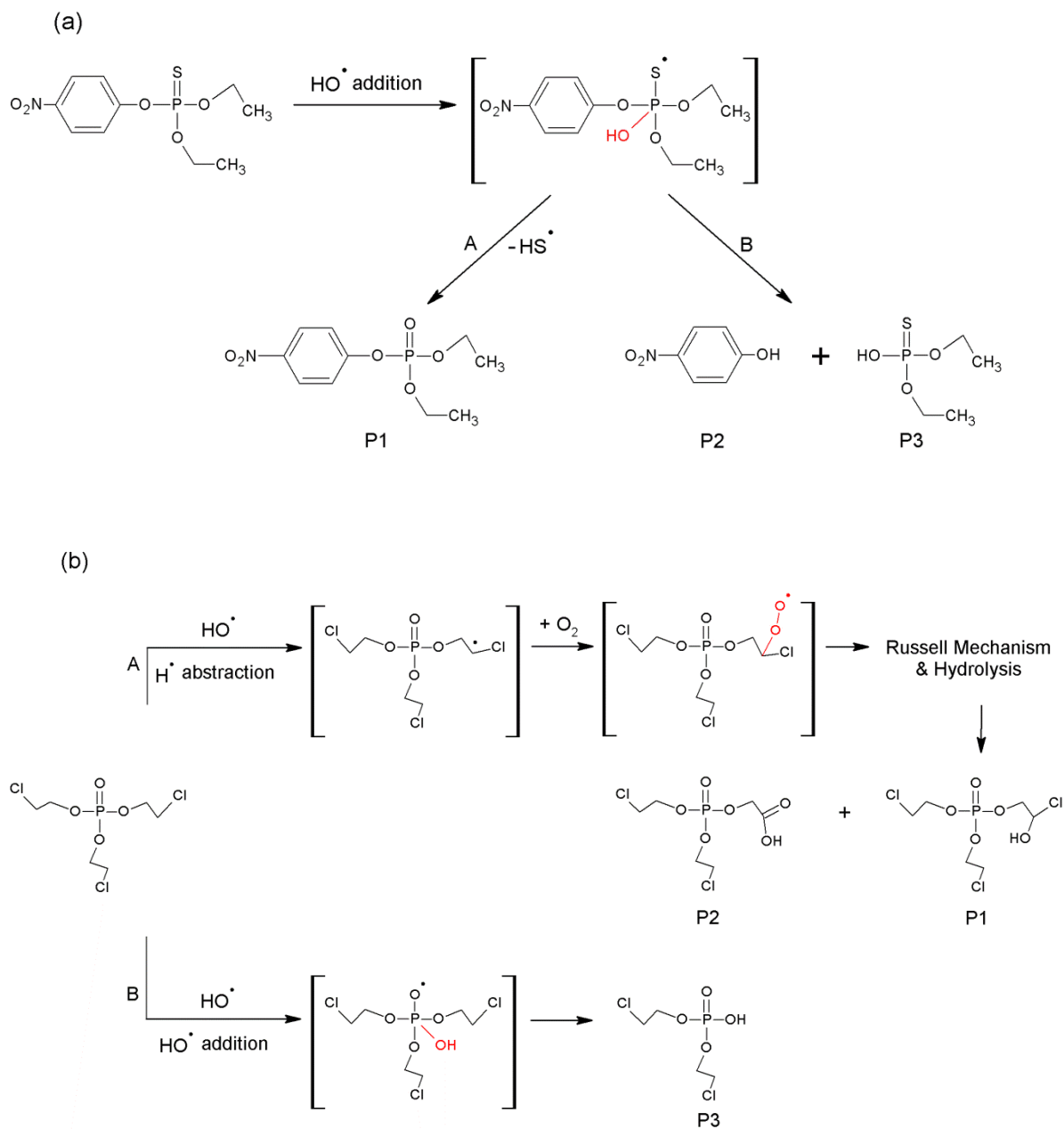


376



377

378 Scheme 2. Proposed transformation mechanisms of OH radical reaction with EP (a) and TCEP

379 (b). Scheme 2a illustrates the rate-limiting step of the photodegradation of EP, which involves

20

380     OH radical addition to the central phosphorus atom and stabilized by two different pathways: (A)

381     the elimination of sulfhydryl radical to produce P=O bond to form paraoxon (P1); (B) the

382     elimination of nitrophenol from the phosphoric center to form P2 and P3. Scheme 2b illustrates

383     the first step reactions of TCEP may simultaneously occur over two different pathways: (A)

384     involves hydrogen abstraction by OH radical, followed by oxygen addition and then undergo

385     Russell Mechanism and hydrolysis to form P1 and P2; (B) involves OH radical addition to the

386     central phosphorus atom, followed by the elimination of an ethyl-chlorine arm from the

387     phosphoric center to form P3.

388     **4. Conclusions**

389     Carbon and hydrogen stable isotope fractionation can be used diagnostically to characterize

390     degradation pathways of phosphates, phosphorothioates and phosphorodithioates which are core

391     structural elements of large variety of OPs. The variation of carbon isotope fractionation pattern

392     has a potential for characterizing different modes of hydrolysis. The hydrogen isotope

393     fractionation is low when a P-O(S) bond in phosphates, phosphorothioates and

394     phosphorodithioates is hydrolyzed. The characteristic isotope fractionation upon hydrolysis may

395     be used for evaluation of remediation approaches using alkaline hydrolysis in contaminated

396     groundwater (LRSB, 2014; Nielsen et al., 2014), whereas the isotope fractionation pattern of the

397     residual fraction may give information about which mode of hydrolysis was at work. The isotope

398     fractionation may be used to characterize hydrolytic reaction in plumes of contaminated aquifers

399     or in the vicinity of industrial dump sites.

400     In case of OH radical oxidation or direct photolysis, cleavage of a C-H bond can lead to a

401     characteristic correlation of hydrogen and carbon fractionation for exploring predominant

402    degradation pathways in surface water bodies or in aerosols. However, phosphorothioates and

403    phosphorodithioates will become desulfurized in the rate limiting step not yielding a larger

404    isotope fractionation which limits the CSIA concept for tracing the process under environmental

405    conditions.  Possible radical oxidation reaction cannot be analyzed by $^2$H and $^{13}$C fractionation

406    when the degradation process is initiated with a desulfurization step in the first irreversible

407    reaction which is a clear limitation for the multi isotope fractionation analysis. Thus, the isotope

408    fractionation might be used for evaluating In Situ Chemical Oxidation (ISCO) of phosphate

409    derivatives but has limitation for phosphorothioates and phosphorodithioates.

410    Hydrolysis and oxidation are concerned to be major degradation pathways for OPs. Our

411    systematic study on $^2$H and $^{13}$C fractionation of OPs shows the potential for analyzing chemical

412    degradation reactions in aquatic environments using the isotope fractionation concept. For

413    further exploring the diagnostic potential of tracing reaction mechanisms in the environment

414    using isotope fractionation, systematic studies on microbial degradation are needed and $^2$H and

415    $^{13}$C fractionation patterns need to be compared with those of chemical transformation reactions.

423   thankful to M. Gehre and S. Kümmel for support in the Isotope Laboratory of the Department of

424   Isotope Biogeochemistry and for the support by the graduate school of the UFZ (HIGRADE).

426   **References**

427   Aguila A, O'Shea KE, Tobien T, Asmus KD. Reactions of hydroxyl radical with dimethyl

428       methylphosphonate and diethyl methylphosphonate. A fundamental mechanistic study. J.

429       Phys. Chem. A 2001; 105: 7834-7839.

430   Andresen JA, Grundmann A, Bester K. Organophosphorus flame retardants and plasticisers in

431       surface waters. Sci. Total. Environ. 2004; 332: 155-66.

432   Araújo TM, Campos MNN, Canela MC. Studying the photochemical fate of methyl parathion in

433       natural waters under tropical conditions. Int. J. Environ. An. Ch. 2007; 87: 937-947.

434   Aston LS, Seiber JN. Exchange of airborne organophosphorus pesticides with pine needles.

435       Journal of Environmental Science and Health Part B 1996; 31: 671-698.

436   Colovic MB, Krstic DZ, Lazarevic-Pasti TD, Bondzic AM, Vasic VM. Acetylcholinesterase

437       inhibitors: pharmacology and toxicology. Curr Neuropharmacol 2013; 11: 315-35.

438   Durand G, Abad JL, Sanchezbaeza F, Messeguer A, Barcelo D. Unequivocal identification of

439       compounds formed in the photodegradation of fenitrothion in water-methanol and

440       proposal of selected transformation pathways. J. Agr. Food Chem. 1994; 42: 814-821.

441   Elsner M. Stable isotope fractionation to investigate natural transformation mechanisms of

442       organic contaminants: principles, prospects and limitations. J. Environ. Monit. 2010; 12:

443       2005-31.

444    Elsner M, Imfeld G. Compound-specific isotope analysis (CSIA) of micropollutants in the

445           environment - current developments and future challenges. Curr. Opin. Biotechnol. 2016;

446           41: 60-72.

447    Elsner M, Jochmann MA, Hofstetter TB, Hunkeler D, Bernstein A, Schmidt TC, et al. Current

448           challenges in compound-specific stable isotope analysis of environmental organic

449           contaminants. Anal. Bioanal. Chem. 2012; 403: 2471-2491.

450    Elsner M, Zwank L, Hunkeler D, Schwarzenbach RP. A New Concept Linking Observable

451           Stable Isotope Fractionation to Transformation Pathways of Organic Pollutants. Environ.

452           Sci. Technol. 2005; 18: 6896–6916.

453    EPA US. Organophosphorus Cumulative Risk Assessment (2006 Update). U.S. Environmental

454           Protection Agency, 2006, pp. 1-189.

455    Evgenidou E, Konstantinou I, Fytianos K, Albanis T. Study of the removal of dichlorvos and

456           dimethoate in a titanium dioxide mediated photocatalytic process through the

457           examination of intermediates and the reaction mechanism. J. Hazard. Mater. 2006; 137:

458           1056-1064.

459    FAO. Parathion-methyl (059). Foog and Agriculture Organization of the United Nations, 1990a.

460    FAO. Parathion (58). Foog and Agriculture Organization of the United Nations, 1990b.

461    Herrmann JM, Guillard C, Arguello M, Aguera A, Tejedor A, Piedra L, et al. Photocatalytic

462           degradation of pesticide pirimiphos-methyl - Determination of the reaction pathway and

463           identification of intermediate products by various analytical methods. Catal. Today 1999;

464           54: 353-367.

465    Hofstetter TB, Berg M. Assessing transformation processes of organic contaminants by

466           compound-specific stable isotope analysis. Trac-trend. Anal. Chem. 2011; 30: 618-627.

467     Hofstetter TB, Spain JC, Nishino SF, Bolotin J, Schwarzenbach RP. Identifying competing

468             aerobic nitrobenzene biodegradation pathways by compound-specific isotope analysis.

469             Environ. Sci. Technol. 2008; 42: 4764-4770.

470     Kanmoni VGG, Daniel S, Raj GAG. Photocatalytic degradation of chlorpyrifos in aqueous

471             suspensions using nanocrystals of ZnO and TiO2. React. Kinet. Mechan. Catal. 2012;

472             106: 325-339.

473     Kawahara J, Horikoshi R, Yamaguchi T, Kumagai K, Yanagisawa Y. Air pollution and young

474             children's inhalation exposure to organophosphorus pesticide in an agricultural

475             community in Japan. Environment International 2005; 31: 1123-1132.

476     Kegley SE, Hill BR, S. O, A.H. C. Methyl parathion  - Identification, toxicity, use, water

477             pollution potential, ecological toxicity and regulatory information. PAN Pesticide

478             Database. Pesticide Action Network, North America, Oakland, CA, 2016a.

479     Kegley SE, Hill BR, S. O, A.H. C. Parathion  - Identification, toxicity, use, water pollution

480             potential, ecological toxicity and regulatory information. PAN Pesticide Database.

481             Pesticide Action Network, North America, Oakland, CA, 2016b.

482     Kerzhentsev M, Guillard C, Herrmann JM, Pichat P. Photocatalytic pollutant removal in water at

483             room temperature: Case study of the total degradation of the insecticide fenitrothion

484             (phosphorothioic acid O,O-dimethyl-O(3-methyl-4-nitro-phenyl) ester). Catal. Today

485             1996; 27: 215-220.

486     Konstantinou IK, Sakellarides TM, Sakkas VA, Albanis TA. Photocatalytic degradation of

487             selected s-triazine herbicides and organophosphorus insecticides over aqueous TiO2

488             suspensions. Environ. Sci. Technol. 2001; 35: 398-405.

489    LRSB L. Pilot experiments on the remediation technology in situ alkaline hydrolysis at Groyne

490        42, Final report. NorthPestClean, Kongens Lyngby, Denmark, 2014.

491    Miyamoto S, Martinez GR, Medeiros MHG, Di Mascio P. Singlet molecular oxygen generated

492        from lipid hydroperoxides by the Russell mechanism: Studies using O-18-labeled linoleic

493        acid hydroperoxide and monomol light emission measurements. J. Am. Chem. Soc. 2003;

494        125: 6172-6179.

495    Nielsen MB, Kjeldsen KU, Lever MA, Ingvorsen K. Survival of prokaryotes in a polluted waste

496        dump during remediation by alkaline hydrolysis. Ecotoxicology 2014; 23: 404-418.

497    Nijenhuis I, Richnow HH. Stable isotope fractionation concepts for characterizing

498        biotransformation of organohalides. Curr. Opin. Biotechnol. 2016; 41: 108-113.

499    Northrop DB. The expression of isotope effects on enzyme-catalyzed reactions. Annual Review

500        of Biochemistry 1981; 50: 103-131.

501    Oshea KE, Beightol S, Garcia I, Aguilar M, Kalen DV, Cooper WJ. Photocatalytic

502        decomposition of organophosphonates in irradiated TiO2 suspensions. J. Photoch.

503        Photobio. A 1997; 107: 221-226.

504    Ou H, Liu J, Ye J, Wang L, Gao N, Ke J. Degradation of tris(2-chloroethyl) phosphate by

505        ultraviolet-persulfate: Kinetics, pathway and intermediate impact on proteome of

506        Escherichia coli. Chem. Eng. J. 2017; 308: 386-395.

507    Pehkonen SO, Zhang Q. The degradation of organophosphorus pesticides in natural waters: A

508        critical review. Crit. Rev. Env. Sci. Tec. 2002; 32: 17-72.

509    Renpenning J, Kuemmel S, Hitzfeld KL, Schimmelmann A, Gehre M. Compound-Specific

510        Hydrogen Isotope Analysis of Heteroatom-Bearing Compounds via Gas

511        Chromatography-Chromium-Based High-Temperature Conversion (Cr/HTC)-Isotope

512        Ratio Mass Spectrometry. Anal. Chem. 2015; 87: 9443-9450.

513    RotterdamConvention. PIC Chemicals - Rotterdam Convention, 2004.

514    Sakellarides TM, Siskos MG, Albanis TA. Photodegradation of selected organophosphorus

515        insecticides under sunlight in different natural waters and soils. Int. J. Environ. An. Ch.

516        2003; 83: 33-50.

517    Santos FF, Martin-Neto L, Airoldi FPS, Rezende MOO. Photochemical behavior of parathion in

518        the presence of humic acids from different origins. J. Environ. Sci. Heal. B 2005; 40:

519        721-730.

520    Singh BK, Walker A. Microbial degradation of organophosphorus compounds. Fems Microbiol.

521        Rev. 2006; 30: 428-471.

522    Stackelberg PE, Gibs J, Furlong ET, Meyer MT, Zaugg SD, Lippincott RL. Efficiency of

523        conventional drinking-water-treatment processes in removal of pharmaceuticals and other

524        organic compounds. Sci. Total. Environ. 2007; 377: 255-72.

525    Thullner M, Centler F, Richnow H-H, Fischer A. Quantification of organic pollutant degradation

526        in contaminated aquifers using compound specific stable isotope analysis – Review of

527        recent developments. Org. Geochem. 2012; 42: 1440-1460.

528    Van Breukelen BM. Extending the Rayleigh equation to allow competing isotope fractionating

529        pathways to improve quantification of biodegradation. Environ. Sci. Technol. 2007; 41:

530        4004-4010.

531    Vogt C, Dorer C, Musat F, Richnow HH. Multi-element isotope fractionation concepts to

532        characterize the biodegradation of hydrocarbons - from enzymes to the environment. Curr.

533        Opin. Biotechnol. 2016; 41: 90-98.

534    Wanamaker EC, Chingas GC, McDougal OM. Parathion hydrolysis revisited: in situ aqueous

535        kinetics by (1)h NMR. Environ. Sci. Technol. 2013; 47: 9267-73.

536    Watts MJ, Linden KG. Photooxidation and subsequent biodegradability of recalcitrant tri-alkyl

537        phosphates TCEP and TBP in water. Water Res. 2008; 42: 4949-54.

538    Watts MJ, Linden KG. Advanced oxidation kinetics of aqueous tri alkyl phosphate flame

539        retardants and plasticizers. Environ. Sci. Technol. 2009; 8: 2937-2942.

540    Wu C, Linden KG. Degradation and byproduct formation of parathion in aqueous solutions by

541        UV and UV/H2O2 treatment. Water Res. 2008; 42: 4780-90.

542    Wu L, Kummel S, Richnow HH. Validation of GC-IRMS techniques for delta13C and delta2H

543        CSIA of organophosphorus compounds and their potential for studying the mode of

544        hydrolysis in the environment. Anal. Bioanal. Chem. 2017; 409: 2581-2590.

545    Wu L, Yao J, Trebse P, Zhang N, Richnow HH. Compound specific isotope analysis of

546        organophosphorus pesticides. Chemosphere 2014; 111: 458-63.

547    Wu LM, White DE, Ye C, Vogt FG, Terfloth GJ, Matsuhashi H. Desulfurization of

548        phosphorothioate oligonucleotides via the sulfur-by-oxygen replacement induced by the

549        hydroxyl radical during negative electrospray ionization mass spectrometry. Journal of

550        Mass Spectrometry 2012; 47: 836-844.

551    Yuan X, Lacorte S, Cristale J, Dantas RF, Sans C, Esplugas S, et al. Removal of

552        organophosphate esters from municipal secondary effluent by ozone and UV/H2O2

553        treatments. Sep. Purif. Technol. 2015; 156: 1028-1034.

554    Zhang N, Schindelka J, Herrmann H, George C, Rosell M, Herrero-Martin S, et al. Investigation

555        of Humic Substance Photosensitized Reactions via Carbon and Hydrogen Isotope

556        Fractionation. Environmental Science & Technology 2015; 49: 233-242.